Development of Real-time Subcellular Dynamic Multicolor Imaging of Cancer-Cell Trafficking in Live Mice with a Variable-Magnification Whole-Mouse Imaging System

Kensuke Yamauchi,[1,2,3] Meng Yang,[1] Ping Jiang,[1] Mingxu Xu,[1] Norio Yamamoto,[3] Hiroyuki Tsuchiya,[3] Katsuro Tomita,[3] Abdool R. Moossa,[2] Michael Bouvet,[2] and Robert M. Hoffman[1,2]

[1]AntiCancer, Inc. and [2]Department of Surgery, University of California, San Diego, California; and [3]Department of Orthopedic Surgery, School of Medicine, Kanazawa University, Takaramachi, Kanazawa, Ishikawa, Japan

Abstract

With the use of dual-color fluorescent cells and a highly sensitive whole-mouse imaging system with both macro-optics and micro-optics, we report here the development of subcellular real-time imaging of cancer cell trafficking in live mice. To observe cytoplasmic and nuclear dynamics in the living mouse, tumor cells were labeled in the nucleus with green fluorescent protein and with red fluorescent protein in the cytoplasm. Dual-color cancer cells were injected by a vascular route in an abdominal skin flap in nude mice. The mice were imaged with an Olympus OV100 whole-mouse imaging system with a sensitive CCD camera and five objective lenses, parcentered and parfocal, enabling imaging from macrocellular to subcellular. We observed the nuclear and cytoplasmic behavior of cancer cells in real time in blood vessels as they moved by various means or adhered to the vessel surface in the abdominal skin flap. During extravasation, real-time dual-color imaging showed that cytoplasmic processes of the cancer cells exited the vessels first, with nuclei following along the cytoplasmic projections. Both cytoplasm and nuclei underwent deformation during extravasation. Different cancer cell lines seemed to strongly vary in their ability to extravasate. With the dual-color cancer cells and the highly sensitive whole-mouse imaging system described here, the subcellular dynamics of cancer metastasis can now be observed in live mice in real time. This imaging technology will enable further understanding of the critical steps of metastasis and provide visible targets for antimetastasis drug development. (Cancer Res 2006; 66(8): 4208-14)

Introduction

Chambers et al. (1) stated that knowledge of metastasis had been limited because it had been a hidden process, which occurs inside the body and was inherently difficult to observe. Chambers' group developed *in vivo* microscopy to overcome this problem using cells labeled with small-molecule fluorescent dyes located on nanospheres (1).

The development of fluorescent proteins to genetically label cells *in vivo* has greatly increased the possibility to observe the metastatic process (2). Our laboratory initially developed the use of green fluorescent protein (GFP) to visualize cancer cells in live tissue (3) and in the intact animal by whole-body imaging (4).

GFP has been used to image movement of cancer cells in live animals. Farina et al. (5) injected GFP-expressing breast cancer cells into the mammary fat pad of female Fischer 344 rats. Metastatic tumor cell movement in live rats was visualized with a laser scanning confocal microscope. Metastatic and nonmetastatic tumor cells were found to differ in their movement. Using multiphoton microscopy, Wang et al. (6) using GFP labeling found five major differences in carcinoma cell behavior between the nonmetastatic and metastatic primary breast tumors involving extracellular matrix, cell motility, and chemotaxis. Goswami et al. (7) have shown that macrophages promote the invasion of GFP-labeled breast cancer cells. However, nuclear-cytoplasmic dynamics could not be visualized in the trafficking cells because the cancer cells were entirely labeled with GFP.

The use of multiple colors for fluorescent protein–based imaging was reported for use in distinguishing tumor cells from host cells (8–11). Multicolor fluorescent proteins were used to distinguish cancer cells from one another (12). Recently, dual-color cancer cells have been developed with GFP in the nuclei and red fluorescent protein (RFP) in the cytoplasm to distinguish cytoplasmic and nuclear behavior in the nucleus (13, 14). To obtain the dual-color cells, RFP was expressed in the cytoplasm of cancer cells, and GFP linked to histone H2B was expressed in the nucleus.

Using the dual-colored cancer cells and a highly sensitive whole-mouse macroimaging/microimaging system, the Olympus OV100, we report here the development of real-time dynamic subcellular imaging of cancer cell trafficking in live mice. In this report, we use this imaging technology to visualize the cytoplasmic and nuclear dynamics of intravascular tumor cell migration and extravasation in live mice.

Materials and Methods

Establishment of dual-color cancer cell lines. To establish dual-color Lewis lung carcinoma (LLC), MMT-060562 murine mammary carcinoma (MMT), and HT-1080 human fibrosarcoma (HT-1080) cells, the cells were transfected with retroviral RFP and histone H2B tagged with H2B-GFP as previously described (5, 6). In brief, the *Hin*dIII/*Not*I fragment from pDsRed2 (Clontech Laboratories, Inc., Palo Alto, CA) was inserted into the *Hin*dIII/*Not*I site of pLNCX2, which also contains the neomycin resistance gene (*neo*®; Clontech Laboratories). For vector production, PT67, an NIH3T3-derived packaging cell line (Clontech Laboratories), was incubated with a precipitated mixture of LipofectAMINE reagent (Life Technologies, Inc., Grand Island, NY) and saturating amounts of pLNCX2-DsRed2 plasmid for 18 hours. For selection of a clone producing high amounts of an RFP retroviral vector (PT67-DsRed2), the cells were cultured in the presence of 200 to 1,000 μg/mol G418 (Life Technologies) for 7 days (10).

The histone *H2B-GFP* fusion gene was inserted at the *Hin*dIII/*Cal*I site of the pLHCX (Clontech Laboratories). To establish a packaging cell clone producing high amounts of histone H2B-GFP retroviral vector, the pLHCX

Note: Supplementary data for this article are available at Cancer Research Online (http://cancerres.aacrjournals.org).

Requests for reprints: Robert M. Hoffman, AntiCancer, Inc., San Diego, CA 92111. Phone: 858-654-2555; Fax: 858-268-4175; E-mail: all@anticancer.com.

doi:10.1158/0008-5472.CAN-05-3927

histone H2B-GFP plasmid containing the hygromycin (HYG) resistance gene (*hyg*®) was transfected in PT67 cells using the same methods described above for PT67-DsRed2. The transfected cells were cultured in the presence of 200 to 400 μg/mL HYG (5).

For RFP and H2B-GFP gene transduction, clones of LLC, MMT, and HT-1080 expressing RFP in the cytoplasm were initially established. The cells were incubated with retroviral supernatants of PT67-RFP cells for 72 hours. Cells were cultured in selective medium, which contained 200 μg/mL G418. The level of G418 was increased stepwise up to 800 μg/mL. The cells were then incubated with retroviral supernatants of PT67-H2B-GFP cells. To select for double transformants, cells were incubated in selective medium with HYG for 72 hours. The level of HYG was increased stepwise up to 400 μg/mL (10).

Mouse model for imaging real-time nuclear-cytoplasmic dynamics of trafficking cancer cells. To image nuclear-cytoplasmic dynamics of trafficking cancer cells in live mice, the dual-color cancer cells were injected into the epigastric cranialis vein. Nude mice were anesthetized with a ketamine mixture (10 μL ketamine HCL, 7.6 μL xylazine, 2.4 μL acepromazine maleate, and 10 μL H_2O) via s.c. injection. An arc-shaped incision was made in the abdominal skin. The s.c. connective tissue was separated to free the skin flap without injuring the epigastrica cranialis artery and vein. The skin flap was spread and fixed on the flat stand. A total of 30 μL medium containing 5×10^5 LLC, MMT, or HT-1080 dual color cell were injected into the epigastrica cranialis vein. For imaging cancer-cell trafficking in blood vessels, images were acquired in real time. For extravasation, images were acquired every hour after injection with the skin flap open or every 12 hours by opening and closing the skin flap (14). The inside surface of the skin flap was directly imaged. A total of 20 mice were used in this study.

Subcellular imaging in live mice. The Olympus OV100 Whole Mouse Imaging System (Olympus Corp., Tokyo, Japan), containing an MT-20 light source (Olympus Biosystems, Planegg, Germany) and DP70 CCD camera (Olympus), was used for subcellular imaging in live mice (Fig. 1). The optics of the OV100 fluorescence imaging system have been specially developed for macroimaging as well as microimaging with high light-gathering capacity. The instrument incorporates a unique combination of high numerical aperture and long working distance. Five individually optimized objective lenses, parcentered and parfocal, provide a 105-fold magnification range for seamless imaging of the entire body down to the subcellular level without disturbing the animal. The OV100 has the lenses mounted on an automated turret with a high magnification range of ×1.6 to ×16 and a field of view ranging from 6.9 to 0.69 mm (Fig. 1*B*). The optics and antireflective coatings ensure optimal imaging of multiplexed fluorescent reporters in small animals. High-resolution images were captured directly on a PC (Fujitsu

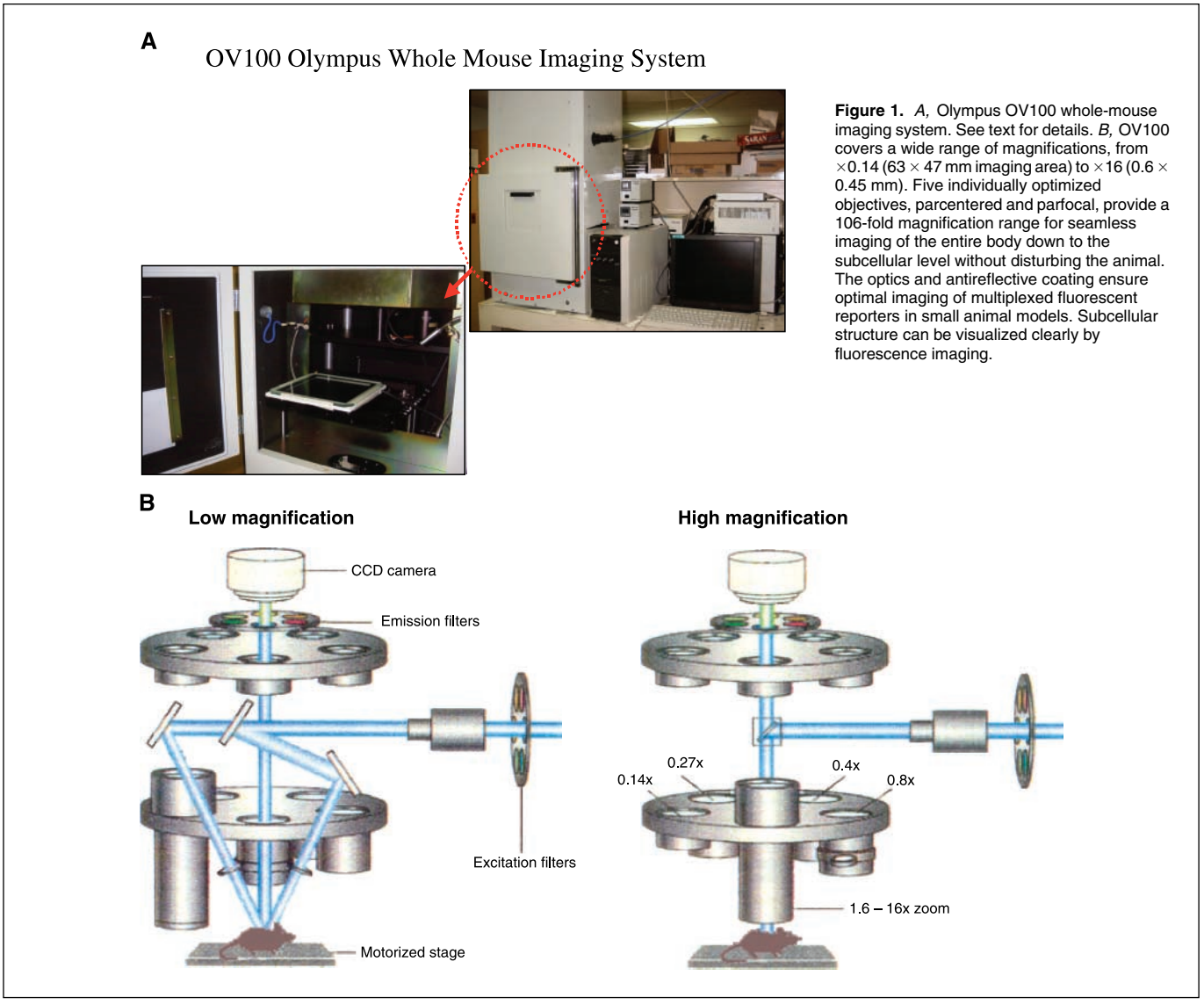

Figure 1. *A,* Olympus OV100 whole-mouse imaging system. See text for details. *B,* OV100 covers a wide range of magnifications, from ×0.14 (63 × 47 mm imaging area) to ×16 (0.6 × 0.45 mm). Five individually optimized objectives, parcentered and parfocal, provide a 106-fold magnification range for seamless imaging of the entire body down to the subcellular level without disturbing the animal. The optics and antireflective coating ensure optimal imaging of multiplexed fluorescent reporters in small animal models. Subcellular structure can be visualized clearly by fluorescence imaging.

Siemens, Munich, Germany). Images were processed for contrast and brightness and analyzed with the use of Paint Shop Pro 8 and Cell^R (Olympus Biosystems; ref. 14).

Mice. Athymic *nu/nu* nude mice were kept in a barrier facility under HEPA filtration. Mice were fed with autoclaved laboratory rodent diet (Tecklad LM-485, Western Research Products, Orange, CA). All animal studies were conducted in accordance with the principals and procedures outlined in the NIH Guide for the Care and Use of Laboratory Animals under assurance no. A3873-1.

Results

Dynamic subcellular imaging of intravascular trafficking of dual-color cancer cells in vessels in live mice. Interaction of cancer cells with blood vessels depends on the ability of the cytoplasm and nucleus to deform, interaction of the cancer cells with endothelial cells, and the diameter of the vessel. Real-time intravascular trafficking of HT1080-GFP-RFP cells was observed in the epigastric vein in a skin flap (Fig. 2*A*) of live mice using the Olympus OV100 whole-mouse imaging system (Fig. 1). The cytoplasm and nuclei were slightly elongated in normal size capillaries (Fig. 2*B*). In a larger vessel, the cells and nuclei remained spherical (Fig. 2*C*). In the larger vessels, some cells attached to the vessel walls. Some of the cells subsequently detached and began crawling on the vessel surface (Fig. 2*C*; see Supplementary Movies S1 and S2). When the cancer cells entered more narrow capillaries, both the whole cell and nucleus were observed to greatly deform by stretching (14). The cytoplasm seems more flexible than the nucleus. When the cancer cells move into capillaries where the diameter is smaller than the deformation limit of the cell, the cancer cell does not advance any further.

The cancer cell velocity depends in part on the size of the vessel. When the cancer cells are migrating in a large capillary, the velocity of the cells averaged 24.2 μm/s (Fig. 2*D*; ref. 14). When the cells went through a narrow capillary, the velocity slowed to an average of 6.1 μm/s (Fig. 2*D*; ref. 14).

Intravascular aggregation of cancer cells is thought to be an important step in metastasis (15). Figure 2*E* shows cancer cell aggregation in a large collecting venule. One aggregate was visualized to collide with another aggregate that was already attached to the vessel wall (Fig. 2*E*). Aggregates sometimes attached to each other. Some aggregates become increasingly larger by repeated collisions. The cellular adhesion in the aggregates is not strong, and some cells escape in the bloodstream (Fig. 2*E*). The double labeling of the nucleus and cytoplasm allowed the distinction of the individual cells and nuclei in the emboli.

Cancer cell adhesion to the endothelium is also important in metastasis (1, 16, 17). Not all cells, however, can attach to the other cancer cells or endothelial cells when they move. Figure 2*C* presents the uncertainty of adhesion. Cancer cell contact with other cancer cells or vessel walls was observed to be frequent. Extravasation was very rare among the HT-1080-GFP-RFP population (see below).

Imaging the dynamics of cancer cell extravasation. MMT-GFP-RFP mouse mammary tumor cells, in contrast to HT-1080 cells, frequently extravasated. MMT-GFP-RFP cells extravasated by first extending cytoplasmic processes (Fig. 3). After cytoplasmic processes were extended, the nuclei followed along the extension undergoing varying degrees of deformation to fit within the extended cytoplasmic protrusion as it left the blood vessel. The whole cell eventually extravasated (Fig. 3*A* and *B*). Extended cytoplasmic processes were frequently observed during extravasation of MMT-GFP-RFP cells. MMT-GFP-RFP cells that initially extravasated remained in proximity of vessels and seemed to surround the vessel (Fig. 3*C*) by 24 hours after injection (see Supplementary Movie S3).

Imaging the fate of post-extravasation cancer cells. Previous studies with the LLC have indicated that these cancer cells adhered to the basement membrane of the lung tissue 24 hours after injection in the tail vein of mice (18). Another study suggested that the time of extravasation of the LLC cells varied in different organs (19). For example, the time of extravasation was 6 hours in the liver and adrenal gland, 16 hours in the lung, and 48 hours in the brain (14). The time of extravasation varied, depending on the structural complexity of the microcirculation in each organ.

In the skin vessels in the present experiments, the extravasated LLC-GFP-RFP cells seemed to stay very closely associated with the vessel. Extravasated LLC-GFP-RFP cells initially migrated along the vessels (Fig. 4*A*), a mechanism termed extravascular migratory metastasis. Lugassy et al. (20) suggested that some melanoma cells were able to migrate along the outside of vessels in a pericyte-like location, forming angiotumoral complexes. We also observed cancer cell division outside of the vessels (Fig. 4*B* and *C, arrows*).

By 120 hours after injection, LLC-GFP-RFP cells were observed to surround a large vessel. Most of the cells were highly elongated, and the major axes of the cells stretched to ~100 μm. The cells and nuclei elongated to occupy as much area as possible on the vessel surface. Rounded premitotic cancer cells on the vessel were observed (Fig. 4*C*). The cancer cells, including their nuclei, elongated and extended their cytoplasmic processes to surround the vessel. The elongated cells seem to round up before cell division, similar to attached cells in culture.

In contrast to the LLC-GFP-RFP and MMT-GFP-RFP carcinoma cells, HT-1080 cells extravasated at a low frequency. HT-1080-GFP-RFP cells did not extend cytoplasmic processes into the host tissue. Occasionally, a cell was observed to divide in a vessel (data not shown), as also observed by Al-Mehdi et al. (21) in static imaging studies. In contrast to the LLC carcinoma and MMT cells, HT-1080-GFP-RFP cells were also observed dying in vessels. Many cells were observed to be dying within vessels by 8 hours after injection. The cells remained round, and cytoplasmic fragmentation was observed in the vessels (data not shown). Even at 24 hours after injection, the majority of the cells remained in vessels without extravasation (data not shown). However, vessels with cancer cells seemed to expand perhaps due to an increase of intravascular pressure (12).

Discussion

Chambers' group was the first to quantify the proportion of injected cancer cells remaining at progressive stages of the metastatic process including: cell arrest in the microcirculation, extravasation, and growth into early micrometastases (1, 16). These authors used cytoplasmic fluorescent nanospheres to label the cells. Cells genetically labeled with fluorescent proteins, especially with multiple colors, offer more possibilities for observing cancer cells in real time in various processes required for metastasis.

Our laboratory introduced the use of GFP for *in vivo* imaging in 1997. With the use of GFP, individual cancer cells could be observed in fresh unstained tissue for the first time (3). In 2000, we showed the first whole-body imaging using GFP (4).

In 2004, we developed cancer cells that were double labeled with GFP in the nucleus and RFP in the cytoplasm (13). With the double-labeled cells, mitotic and apoptotic cells were imaged in live animals. We also imaged cancer cells that underwent cytoplasmic

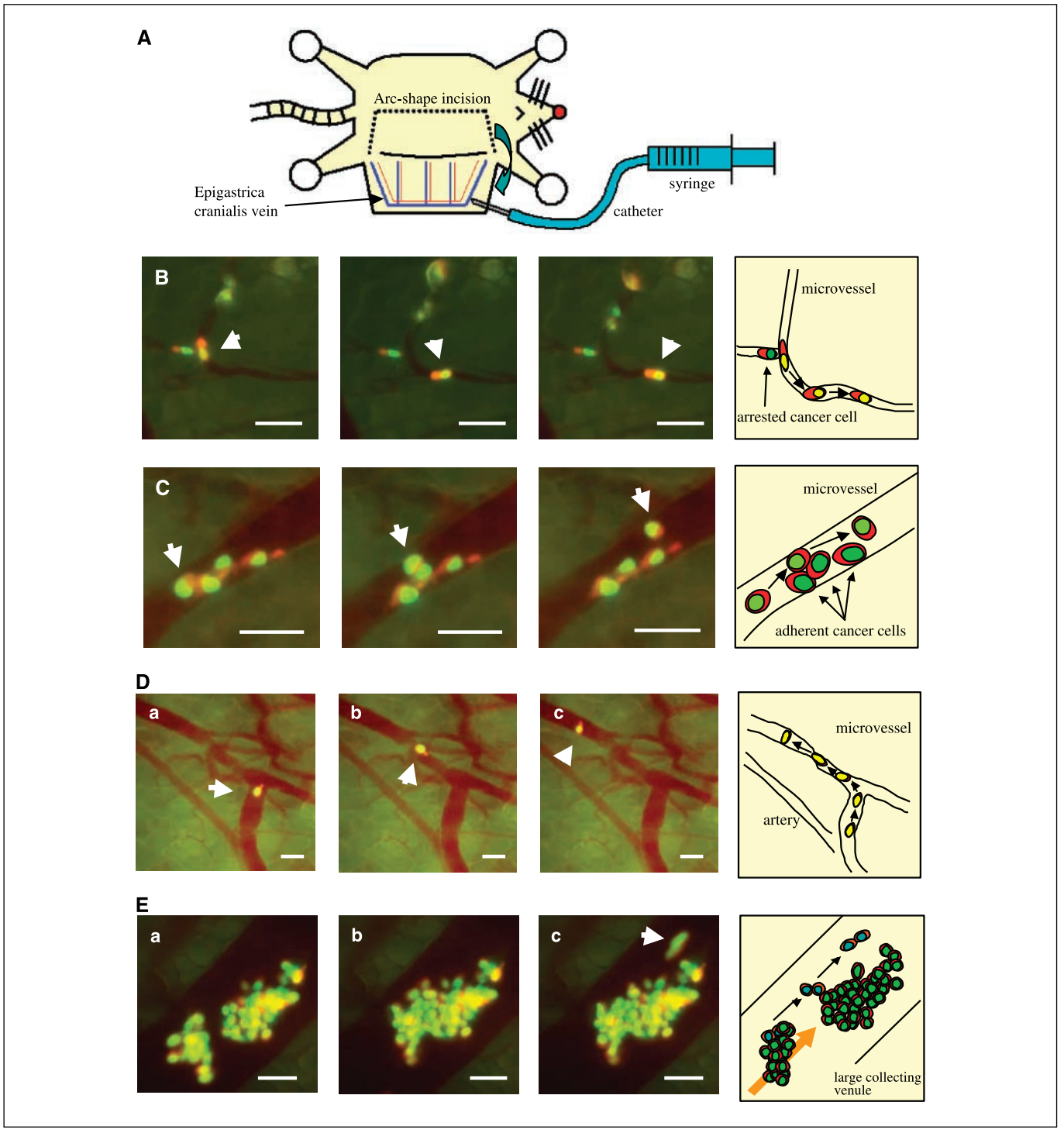

Figure 2. Intravascular trafficking of dual-color HT-1080 human fibrosarcoma cells labeled in the nucleus with histone H2B-GFP and in the cytoplasm with RFP. *A,* schematic diagram of the skin flap model in live mice for imaging intravascular trafficking and extravasation. An arc-shaped incision was made in the abdominal skin, and then the skin flap was spread and fixed on a flat stand. Dual-color HT-1080 cells are injected into the epigastrica cranialis vein through a catheter. Immediately after injection, the inside surface of the skin flap was directly observed. *B,* dual-color HT-1080 cell crawls smoothly along the vessel wall without rolling in a capillary (*arrow*). The nucleus and cytoplasm are slightly stretched. The nucleus is in the front of the cell while the cell is crawling. When the cell advances into a part of the capillary where the diameter is smaller than of deformation limit of the cell, the cell does not advance any further. Bar, 100 μm. *C,* dual-color HT-1080 cell, trafficking at low velocity, advances between other cells and the vessel wall. The moving cancer cell contacts the other cells (*arrow*). The cell deforms slightly and continues to move without adhesion. Bar, 100 μm. *Right,* schematics of (*B*) and (*C*). *D,* One cancer cell migrating in the post capillary with slow velocity. The cytoplasm is at the head of the cell while the cell is moving in a large vein, but the nucleus is at the head in a small vein. The velocity of the cells in (*A*) and (*B*) is an average of 24.2 μm/s. The average velocity in cells in (*D*) and (*E*), however, is only 6.1 μm/s because the cells are in a narrower vein. Images were taken every 3.30 seconds. Bar, 50 μm. *E,* multicellular aggregate collides with another aggregate that is already attached to the vessel wall. The two aggregates attach and form a larger aggregation. Some cells (*arrow*) escape from the aggregate because of weak adhesion and recommence movement. Images were taken every 1.04 seconds. Bar, 100 μm. Images were acquired in real time with the Olympus OV100. *Right,* schematics of (*B*) and (*C*).

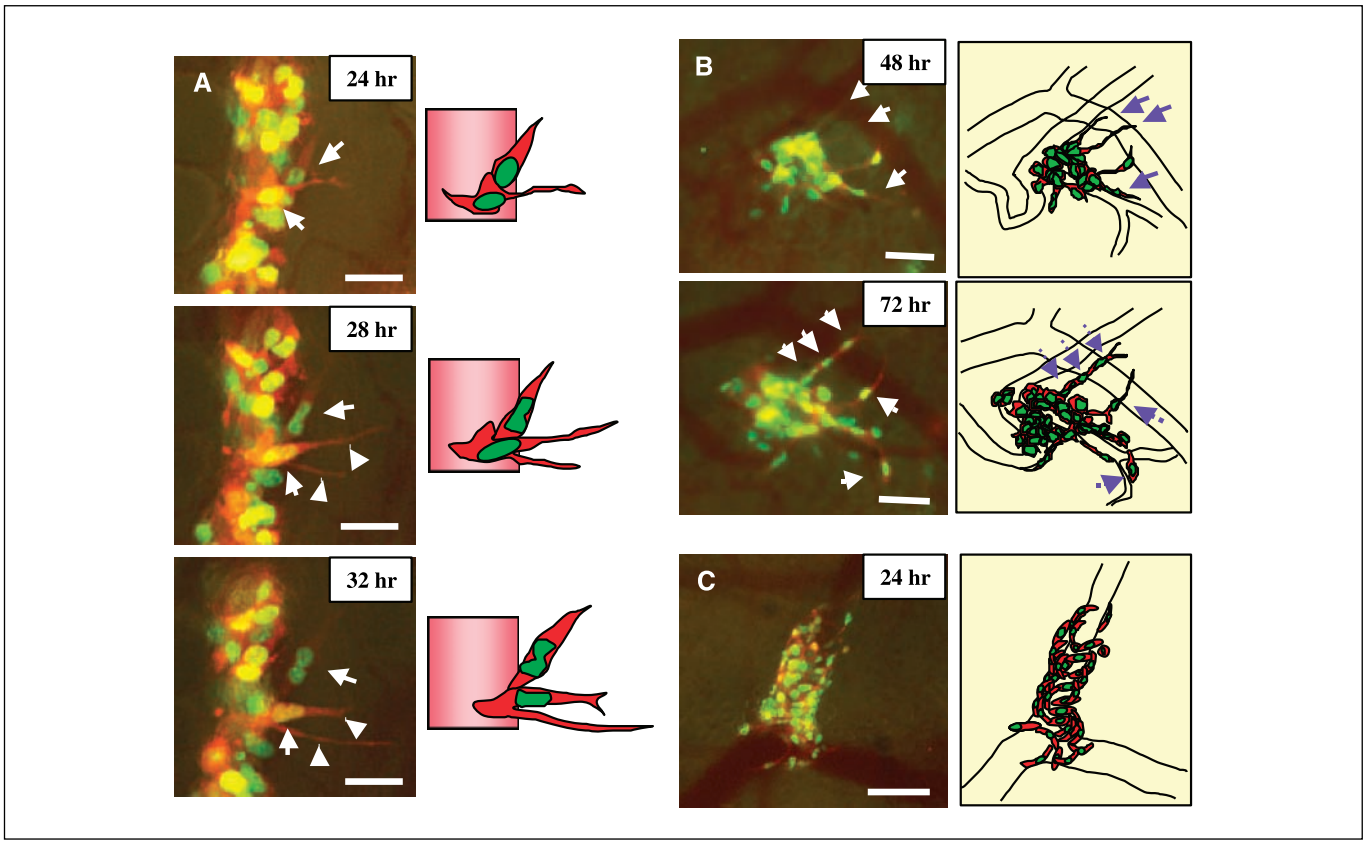

Figure 3. Time-lapse imaging of extravasation of dual-color MMT mouse mammary tumor cells. *A,* 12 hours after injection, the skin flap is opened and fixed on a flat stand as described in Fig. 2. Images are acquired every hour for 24 hours with the skin flap open. Two MMT cells are visualized in the process of extravasation 24 hours after injection (*arrows*). The cancer cells extend fine cytoplasmic projections into the host tissue at the onset of extravasation. One of the cells extends two fine cytoplasmic projections into the host tissue (*arrowhead*). The nuclei then migrate along the cytoplasmic projection until the whole cell is out of the vessel. Subsequently, the whole cell extravasates. Bar, 20 μm. *B,* 48 and 72 hours after injection as in Fig. 2*A*. Cytoplasmic processes are extended along the vessel wall 48 hours after injection (*arrows*). Cells extravasate in the same direction of the cytoplasmic projections (*broken arrows*). Images were acquired every 24 hours by opening and closing the skin flap. Bar, 50 μm. *C,* invasion and proliferation of MMT cells around a vessel after extravasation. Bar, 50 μm. Images were acquired with the Olympus OV100. *Right,* schematics of (*A*), (*B*), and (*C*).

and nuclear deformation in small capillaries in the brain in the live animal (13).

In 2005, using the dual-color cancer cells, we imaged and quantified the maximum nuclear and cytoplasmic deformation of cancer cells in small capillaries after injection in the heart. We observed that the whole cancer cell could stretch to four times its original length to fit in a small capillary, whereas the nucleus could stretch only to ~1.6 times its original length. After injection of dual-color cancer cells, the velocity of cancer cell movement was roughly estimated by acquiring an image of the cancer cells in small capillaries at one time point and then imaging them in the same capillary 2 hours later (14).

In the present study, in contrast to previous studies with periodic imaging, dual-color cancer cells were continuously imaged in both large and small vessels in the live mouse. Rather than heart injection as was done previously, dual-color cancer cells were directly injected in the vessel to be observed. Using a variable magnification whole-mouse imaging system, images were continuously acquired of cancer cells trafficking in various size vessels for relatively long periods of time. Cancer cell behavior that previously was only inferred from either fixed preparations, single images, or single-color video images was now observed in dual-color to distinguish cytoplasm and nucleus. For example, cancer cells were observed as they crawled on blood vessel walls, rolled along the vessel walls, or as they detached and were swept along with the blood flow. Nuclear and cytoplasmic shape changes were continuously observed during these processes. Large shape changes both in the nucleus and the cytoplasm were observed as the cancer cells moved from a larger to a smaller vessel. The formation of emboli could be continuously observed such that the individual cells within the emboli were readily distinguished because the nuclei and cytoplasm were differentially labeled. Other cell-cell interactions were observed. For example, cancer cells bumping into each other, sometimes attaching to each other, or sometimes dislodging an attached cell from the vessel wall or from an embolus. Some cancer cells seemed to be able to directly avoid other cancer cells in small vessels as they continually crawled along the vessel wall. The crawling cancer cells were observed either to move with the nucleus in the front of the cell, whereas at other times the nucleus was in the rear. The ability to continuously observe cancer nuclear and cytoplasmic dynamics during trafficking will allow a much deeper understanding of how cancer cells spread in the body in different size vessels. In addition, the ability to continuously image cancer-cell nuclear and cytoplasmic dynamics provides visible targets for screening of drugs that can inhibit the various types of cancer cell movement.

In the present study, the nuclear and cytoplasmic behavior of the dual-color cancer cells was observed in real time and time lapse in

the live animal during the extravasation process. Some cancer cell lines were observed to extravasate well, such as the MMT breast cancer cell line. Cytoplasmic processes of dual-color cancer cells were observed to form what seemed to be pores in the vessel wall through which they exited. The nuclei flowed along the cytoplasmic processes, which made the pore and subsequently the entire cell finally will extravasate. Other cancer cells were observed to follow through the pore. In contrast, HT-1080 cells, although they migrated very efficiently in blood vessels, only rarely were they observed to extravasate. The ability to continuously image the complex behavior of the nucleus and cytoplasm during extravasation will also provide new visible drug targets to inhibit this critical step of metastasis.

Post-extravasation behavior was also imaged in the MMT cells as well as the LLC cells. These cells adhered in large numbers on the outer surface of the vessel wall after extravasation and subsequently proliferated on the outer surface of the vessel. Cancer cell proliferation on the vessel surface was so extensive they seemed to form a confluent monolayer. The cancer cells seemed to take advantage of the vessel surface to obtain nutrients and oxygen. This behavior of the cancer cells adds a new dimension to our understanding of angiogenesis. Not only do vessels act as a conduit for cancer cell movement throughout the cell body and provide cancer cells in the parenchyma with nutrients and oxygen, they also act as a substrate on which cancer cells can extensively proliferate. LLC cells seem most adept in growing on the vessel surface with cells and nuclei stretching as if they were on a Petri dish surface. Dual-color mitotic cells were observed to round up and divide on the vessel surface.

With the ability to continuously image cancer cells at the subcellular level in the live animal, our understanding of the complex steps of metastasis will significantly increase. In addition, new drugs can be developed to target these newly visible steps of metastasis.

Conclusions

The dual-color cancer cells and the Olympus OV100 whole-mouse imaging system used in the present study enable real-time subcellular dynamic imaging of cancer cells in the live mouse. With this new imaging technology, we were able to observe, with very high resolution, nuclear and cytoplasmic dynamics during intravascular cancer trafficking and extravasation.

The skin flap model used in this study has important advantages for observation of metastatic process at the subcellular level. For example, the skin can be spread stably on a stand such that the motion from the mouse's heartbeat or breathing has no influence on acquisition of images. Disturbance of the skin blood supply does not occur during the skin flap procedure. In addition, the skin flap could be completely reversed such that the mice need not be sacrificed and could be observed at subsequent time periods.

The dual-color cells enabled the observation of the nuclear-cytoplasmic dynamics of the cancer cells during cell migration and extravasation. In these processes, single dual-color cells could be distinguished in emboli as they are formed or as cells escape from them. Nuclear GFP expression enabled visualization of nuclear dynamics; cytoplasmic RFP expression enabled visualization of cytoplasmic dynamics in these processes. The ability to make these observations was especially important in extravasation.

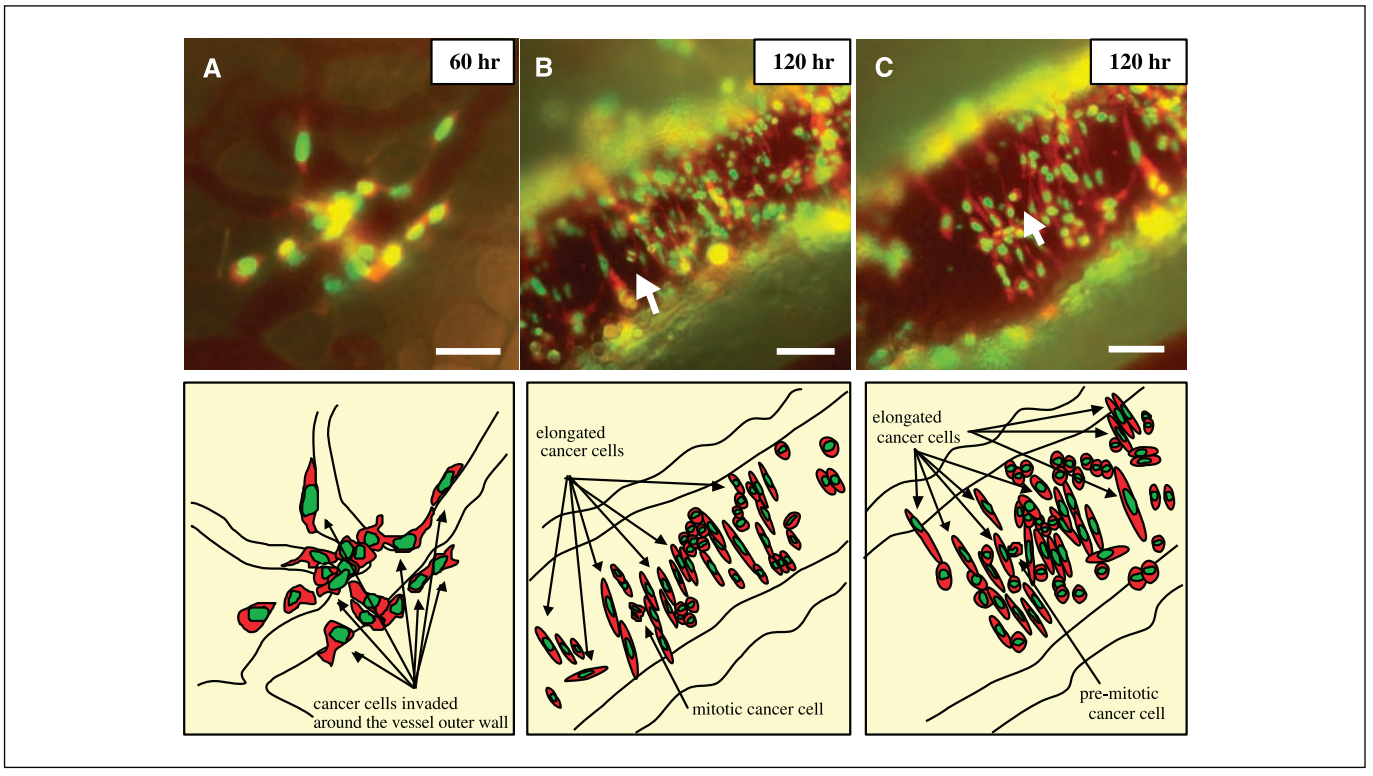

Figure 4. Imaging of extravasation, invasion, and proliferation of dual-color LLC cells. *A,* LLC cells are observed to proliferate on the vessel outer wall 60 hours after injection. *B* and *C,* extravasated LLC cells wind around a large vessel 120 hours after injection. Most of the cells and nuclei are elongated with the major axes of the cells reaching ~100 μm. Mitotic and premitotic cancer cells round up and nuclei are condensed. Bar, 100 μm. Images were acquired with the Olympus OV100. *Bottom,* schematics of (*A*), (*B*), and (*C*).

We showed major differences in the ability to extravasate among three cancer cell lines observed in the present study. The LLC cells and MMT cells could extravasate and form large metastatic colonies on the outer surface of the vessel. During the extravasation process, MMT GFP-RFP cells produced elongated cytoplasmic processes, which extended into the host tissue. Nuclei deformed to exit the vessel within the extended cytoplasmic processes. Extravasation of these cells took ~24 hours. After extravasation, some cells migrated along the outside of the vessels and eventually surrounded or stayed in proximity to the vessels. The extravasated LLC-GFP-RFP cells subsequently surround the blood vessels, deformed to occupy as much surface area as possible, and proceeded to extensively divide using the outer vessel surface as a substrate. HT-1080-GFP-RFP cells, on the other hand, extravasated very infrequently. Most of the HT-1080-GFP-RFP cells still remained in vessels 96 hours after injection, without extension of the cytoplasmic processes into the host tissue. These data suggest that extravasation, an early step in hematogenous metastasis, varies significantly in different cancer cell lines. The ability to extravasate and invade seems to involve both cytoplasmic and nuclear properties.

The *in vivo* GFP imaging technology described in this report should lead to much deeper understanding of the mechanisms of cancer cell invasion and metastasis at the cellular and subcellular levels as well as provide new visible targets for drug therapy.

Acknowledgments

Received 11/1/2005; revised 1/27/2006; accepted 2/8/2006.

Grant support: National Cancer Institute grants CA099258 (AntiCancer), CA103563 (AntiCancer), CA101600 (AntiCancer), and R21 CA109949-01 (M. Bouvet) and American Cancer Society grant RSG-05-037-01-CCE (M. Bouvet).

The costs of publication of this article were defrayed in part by the payment of page charges. This article must therefore be hereby marked *advertisement* in accordance with 18 U.S.C. Section 1734 solely to indicate this fact.

References

1. Chambers AF, Groom AC, Macdonald IC. Dissemination and growth of cancer cells in metastatic sites. Nat Rev Cancer 2002;2:563–72.

2. Hoffman RM. The multiple uses of fluorescent proteins to visualize cancer *in vivo*. Nat Rev Cancer 2005;5:796–806.

3. Chishima T, Miyagi Y, Wang X, et al. Cancer invasion and micrometastasis visualized in live tissue by green fluorescent protein expression. Cancer Res 1997;57:2042–7.

4. Yang M, Baranov E, Jiang P, et al. Whole-body optical imaging of green fluorescent protein-expressing tumors and metastases. Proc Natl Acad Sci U S A 2000;97:1206–11.

5. Farina KL, Wyckoff JB, Rivera J, et al. Cell motility of tumor cells visualized in living intact primary tumors using green fluorescent protein. Cancer Res 1998;58:2528–32.

6. Wang W, Wyckoff JB, Frohlich VC, et al. Single cell behavior in metastatic primary mammary tumors correlated with gene expression patterns revealed by molecular profiling. Cancer Res 2002;62:6278–88.

7. Goswami S, Sahai E, Wyckoff JB, et al. Macrophages promote the invasion of breast carcinoma cells via a colony-stimulating factor-1/epidermal growth factor paracrine loop. Cancer Res 2005;65:5278–83.

8. Yang M, Li L, Jiang P, Moossa AR, Penman S, Hoffman RM. Dual-color fluorescence imaging distinguishes tumor cells from induced host angiogenic vessels and stromal cells. Proc Natl Acad Sci U S A 2003;100:14259–62.

9. Yang M, Reynoso J, Jiang P, Li L, Moossa AR, Hoffman RM. Transgenic nude mouse with ubiquitous green fluorescent protein expression as a host for human tumors. Cancer Res 2004;64:8651–6.

10. Amoh Y, Li L, Yang M, et al. Hair follicle-derived blood vessels vascularize tumors in skin and are inhibited by doxorubicin. Cancer Res 2005;65:2337–43.

11. Kaplan RN, Diba RD, Zacharoulis S, et al. VEGFR1-positive haematopoietic bone marrow progenitors initiate the pre-metastatic niche. Nature 2005;438:820–7.

12. Yamamoto N, Yang M, Jiang P, et al. Determination of clonality of metastasis by cell-specific color-coded fluorescent-protein imaging. Cancer Res 2003;63:7785–90.

13. Yamamoto N, Jiang P, Yang M, et al. Cellular dynamics visualized in live cells *in vitro* and *in vivo* by differential dual-color nuclear-cytoplasmic fluorescent-protein expression. Cancer Res 2004;64:4251–6.

14. Yamauchi K, Yang M, Jiang P, et al. Real-time *in vivo* dual-color imaging of intracapillary cancer cell and nucleus deformation and migration. Cancer Res 2005;65:4246–52.

15. Leighton J. The spread of cancer. Pathogenesis, experimental methods, interpretations. New York: Academic Press; 1967.

16. Luzzi KJ, Macdonald IC, Schmidt EE, et al. Multistep nature of metastasis inefficiency: dormancy of solitary cells after successful extravasation and limited survival of early micrometastasis. Am J Pathol 1998;153:865–73.

17. Paku S, Dome B, Toth R, Timar J. Organ-specificity of the extravasation process: an ultrastructural study. Clin Exp Metastasis 2000;18:481–92.

18. Koop S, Macdonald IC, Luzi K, et al. Fate of melanoma cells entering the microcirculation: over 80% survive and extravasate. Cancer Res 1995;55:2520–3.

19. Kim YK, Borsig L, Han HL, Varki NM, Varki A. Distinct selectin ligands on colon carcinoma mucins can mediate pathological interactions among platelets, leukocytes, and endothelium. Am J Pathol 1999;155:461–72.

20. Lugassy C, Kleinman HK, Engbring JA, et al. Pericyte-like location of GFP-tagged melanoma cells: *ex vivo* and *in vivo* studies of extravascular migratory metastasis. Am J Pathol 2004;164:1191–8.

21. Al-Mehdi AB, Tozawa K, Fisher AB, Shientag L, Lee A, Muschel RJ. Intravascular origin of metastasis from the proliferation of endothelium-attached tumor cells: a new model for metastasis. Nat Med 2000;6:100–2.